CrystEngComm

ROYAL SOCIETY OF CHEMISTRY

COMMUNICATION

View Article Online
View Journal | View Issue

Cite this: *CrystEngComm*, 2023, **25**, 2990

Received 4th February 2023,
Accepted 11th April 2023

DOI: 10.1039/d3ce00106g

rsc.li/crystengcomm

Selective synthesis of two-dimensional semiconductive coordination polymers with silver–sulfur network†

Ryohei Akiyoshi, [a] Akinori Saeki, [b] Kazuyoshi Ogasawara,[a] Hirofumi Yoshikawa, [c] Yuiga Nakamura [d] and Daisuke Tanaka *[a]

Two-dimensional Ag(I) coordination polymers containing a sulfur coordination atom, $[Ag(tzdt)]_n$ (KGF-24), and $[Ag(tzdt)(TFA)]_n$ (KGF-25) (Htzdt = 1,3-thiazolidine-2-thione, TFA = trifluoroacetate), were synthesized and characterized. Time-resolved microwave conductivity measurements and first-principles calculations revealed that KGF-24 and KGF-25 exhibit charge mobility along their $(–Ag–S–)_n$ network.

Electrically conductive coordination polymers (CPs) and metal–organic frameworks (MOFs)[1] are attracting increasing attention because of their use in a wide range of applications such as electrocatalysis,[2] chemiresistive sensing,[3] and energy storage materials.[4] In particular, sulfur-coordinated CPs (S-CPs) comprising $(–M–S–)_n$ networks have been extensively investigated in recent years because of their excellent potential electrical conductivities and semiconducting properties resulting from charge delocalization through their infinite $(–M–S–)_n$ structure.[5] In these systems, the metal ion species and structural dimensionalities of the inorganic $(–M–S–)_n$ moiety of S-CPs significantly influence their electronic properties, including the band gap and charge mobility.[5b,c,6]

Among the various S-CPs, two-dimensional (2D) Ag(I)-based S-CPs composed of a $(–Ag–S–)_n$ structure show remarkable charge-transport properties.[7] For example, 2D Ag(I) S-CPs with benzenethiol (HSPh) derivatives $[Ag(SPhX)]_n$ (X = COOH, F, OCH_3, OH, and NH_2) exhibit high hole mobility along their 2D-extended inorganic $(–Ag–S–)_n$ structure. Hence, they are utilized for chemiresistive gas sensing.[7b,c] Although 2D Ag(I) S-CPs are promising semiconductor materials that exhibit excellent electronic performance, they have been mainly investigated using monodentate sulfur-based ligands such as HSPh[7b–g] and alkanethiol[8] derivatives. In addition, their structural diversity is still limited.

This study focuses on the 1,3-thiazolidine-2-thione (Htzdt) ligand comprising a five-membered ring containing N and S atoms along with a thiol substituent. Huang *et al.* have shown that the Ag(I) S-CPs based on an Htzdt ligand can form one-, two-, and three-dimensional (*i.e.*, 1D, 2D, and 3D) architectures comprising $(–Ag–S–)_n$ network.[9] However, the electronic properties of these S-CPs are yet to be explored despite their excellent semiconducting property.

Motivated in part by the aforementioned studies, we herein investigate the semiconductive property of 2D Ag(I) S-CP $[Ag(tzdt)]_n$ (denoted as **KGF-24**). Further, we synthesize a new 2D Ag(I) S-CP containing the Htzdt ligand, $[Ag_2(tzdt)(TFA)]_n$ (denoted as **KGF-25**; TFA = trifluoroacetate), and characterize its semiconductive characteristics (Scheme 1). Both **KGF-24** and **KGF-25** exhibited photoconductivity along their 2D-extended structures composed of the $(–Ag–S–)_n$ network.

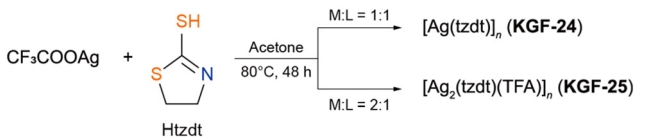

Scheme 1 Selective synthesis of $[Ag(tzdt)]_n$ (**KGF-24**) and $[Ag_2(tzdt)(TFA)]_n$ (**KGF-25**) using CF_3COOAg (M) and Htzdt (L). Synthesis at an M : L ratio of 1 : 1 gives rise to **KGF-24**, while yielding **KGF-25** at an M : L ratio of 2 : 1.

[a] *Department of Chemistry, School of Science, Kwansei Gakuin University, 1 Gakuen Uegahara, Sanda, Hyogo 669-1330, Japan. E-mail: dtanaka@kwansei.ac.jp*
[b] *Department of Applied Chemistry, Graduate School of Engineering, Osaka University, 2-1 Yamadaoka, Suita, Osaka 565-0871, Japan*
[c] *Department of Nanotechnology for Suitable Energy, School of Engineering, Kwansei Gakuin University, 1 Gakuen Uegahara, Sanda, Hyogo 669-1330, Japan*
[d] *Japan Synchrotron Radiation Research Institute (JASRI), 1-1-1 Kouto, Sayo-cho, Sayo-gun, Hyogo 679-5198, Japan*

† Electronic supplementary information (ESI) available: Experimental section, SEM textures, crystallographic data, asymmetric unit, structure around Ag(I) center, packing of 2D structure, simulated and experimental PXRD patterns, TG analysis data, PXRD patterns after thermal decomposition, PYS results, list of TRMC results, excitation laser intensities dependent TRMC results, distribution of VBM and CBM. CCDC 2236352 and 2236353. For ESI and crystallographic data in CIF or other electronic format see DOI: https://doi.org/10.1039/d3ce00106g

KGF-24 and **KGF-25** were prepared by solvothermal synthesis in an autoclave using CF_3COOAg (M) and Htzdt (L) at M : L ratios of 1 : 1 for **KGF-24** and 2 : 1 for **KGF-25** (see the Experimental section in the ESI†). Scanning electron microscopy (SEM) images indicate that both compounds were obtained as plate crystals (Fig. S1†). The respective crystal structures were determined by single-crystal X-ray diffraction. The crystal parameters are shown in Table S1.† The full structural data can be obtained from the CCDC (2236352 and 2236353). **KGF-24** crystalized in the monoclinic $P2_1/c$ space group, consistent with the previously reported literature.[9b] The asymmetric unit was composed of a Ag(I) ion and deprotonated $tzdt^-$ anion (Fig. S2a†), wherein the Ag(I) center was coordinated by two S1 atoms and one N atom derived from $tzdt^-$ ligands, forming an $[AgS_2N]$ planar coordination structure (Fig. S3a†). The Ag–S bond lengths were 2.45 and 2.71 Å, and the Ag–N bond length was 2.20 Å. The N and S1 atoms of $tzdt^-$ bridged two Ag(I) centers to yield a dinuclear unit with an Ag–Ag bond of 2.90 Å (Fig. 1a). The Ag–Ag bond could be attributed to the close-shell d^{10}–d^{10} interaction.[10] The S1 atom of $tzdt^-$ also serves as a μ_2-S atom to further connect dinuclear units, thus forming a 2D structure with an interlayer distance of 10.8 Å (Fig. 1b and c and S4a†). Notably, the 2D architecture comprises a 1D-extended $[–Ag–S–]_n$ structure (Fig. 1d).

Similar to **KGF-24**, **KGF-25** crystallized in the monoclinic $P2_1/c$ space group, in which the asymmetric unit contained two crystallographically non-equivalent Ag(I) ions (Ag1 and Ag2), one deprotonated $tzdt^-$ anion, and one TFA^- anion (Fig. S2b†). Both the Ag1 and Ag2 centers adopt 4-fold coordination structures with $[Ag1S_2NO]$ and $[Ag2S_3O]$ donor sets, respectively (Fig. S3b†). The TFA^- was bi-dentate, bound to Ag1 and Ag2. The S2 atom of the $tzdt^-$ ring and the S1 atom derived from the thiolate behave as coordination

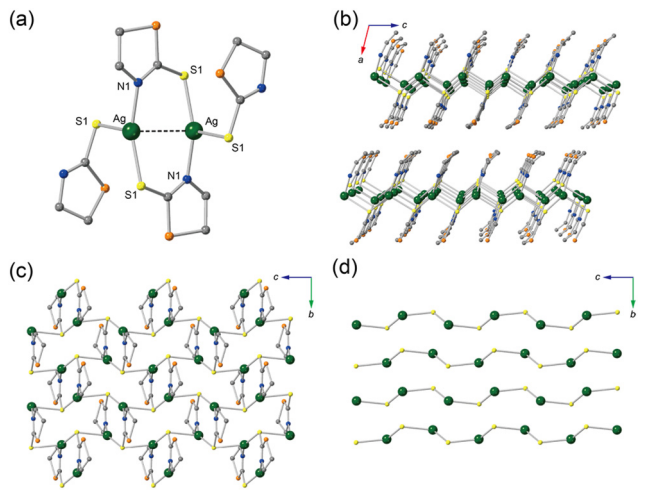

Fig. 1 Crystal structure of **KGF-24**. (a) Dinuclear coordination unit. Ag–Ag bond is shown by the dashed black line. (b) Packing of the 2D layer structure. (c) 2D layer structure parallel to the *bc* plane. (d) $(–Ag–S–)_n$ network in the 2D layer structure. Color code: Ag; dark green, S1; yellow, S2; orange, N; blue, C; gray. H atoms are omitted for clarity.

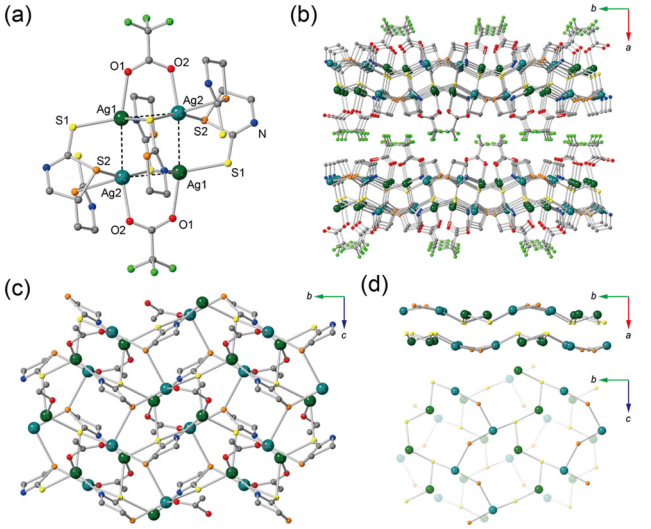

Fig. 2 Crystal structure of **KGF-25**. (a) Tetranuclear coordination unit. Ag–Ag bond is shown by the dashed black line. (b) Packing structure along the *c*-axis. (c) 2D layer structure parallel to the *bc* plane. F atoms are omitted for clarity. (d) $(–Ag–S–)_n$ network in the 2D layer structure. Color code: Ag1; dark green, Ag2; teal blue, S1; yellow, S2; orange, N; blue, C; gray, O; oxygen, F; light green. H atoms are omitted for clarity.

atoms, forming a tetranuclear coordination unit (Fig. 2a). In this tetranuclear unit, Ag–Ag bonds resulting from close-shell d^{10}–d^{10} interactions were observed (Ag1–Ag2 = 2.95 and 3.06 Å). The S1 and S2 atoms respectively act as μ_3-S and μ_2-S that connect the adjacent tetranuclear coordination units, forming a 2D layer parallel to the *ac* plane (Fig. 2b and c). The 2D layers have an interlayer distance of 12.4 Å, which is larger than that of **KGF-24** because of the presence of the bulky TFA^- anion (Fig. S4b†). In the $(–Ag–S–)_n$ structure, the 2D structure of **KGF-25** consists of two $(–Ag–S–)_n$ layers composed of alternatively aligned $(–Ag1–S1–)_n$ and $(–Ag2–S2–)_n$ chains (Fig. 2d).

Collectively, complexation between CF_3COOAg and Htzdt produced two kinds of 2D Ag(I) S-CPs depending on the M : L ratio. **KGF-24** showed the formation of 2D structures composed of $[AgS_2N]$ coordination units, which is consistent with the previously reported literature.[9b] In contrast, **KGF-25** formed 2D architectures comprising $[Ag1S_2NO]$ and $[Ag2S_3O]$ coordination units. Notably, the 2D structures comprised a 1D-extended $(–Ag–S–)_n$ chain for **KGF-24** and 2D-extended $(–Ag–S–)_n$ layer for **KGF-25**. The purities of **KGF-24** and **KGF-25** were confirmed by elemental analyses and powder X-ray diffraction (PXRD) (Fig. S5†).

The thermal stabilities of **KGF-24** and **KGF-25** were examined by thermogravimetry (TG) analysis. As shown in Fig. S6,† the structures of **KGF-24** and **KGF-25** were stable up to ~170 °C under N_2 atmosphere. Upon further heating to over 200 °C, both compounds mainly decomposed to Ag_2S, as corroborated by PXRD measurements (Fig. S7†).

The electronic properties and optical band gap energies of **KGF-24** and **KGF-25** were investigated through diffuse-

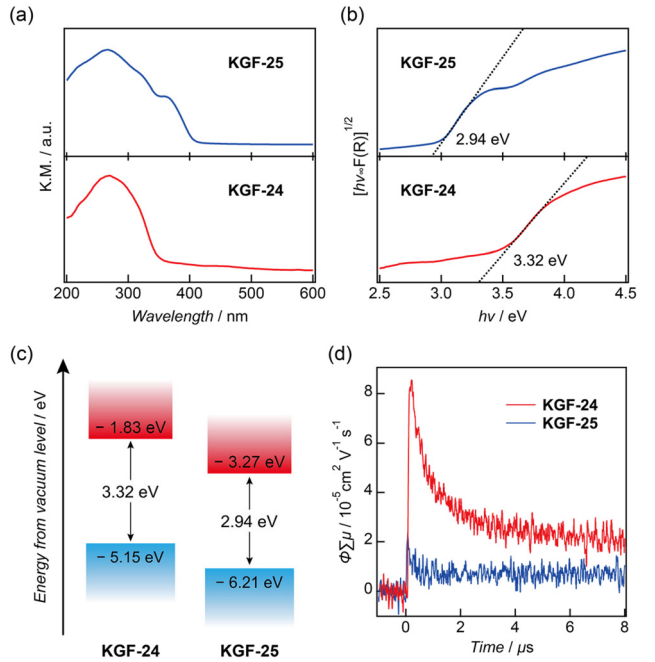

Fig. 3 Semiconductive properties of **KGF-24** and **KGF-25**. (a) DR-UV-vis spectroscopy. (b) Tauc plot. (c) Energy diagram below vacuum level. VBM energy level was determined by PYS experiments as depicted in Fig. S7.† (d) Results of TRMC experiments (λ_{ex} = 355 nm; red: **KGF-24**, blue: **KGF-25**).

reflectance ultraviolet-visible (DR-UV-vis) spectroscopy. As presented in Fig. 3a, **KGF-24** and **KGF-25** display absorption maxima centered at ~269 and 266 nm, respectively. The optical band gaps were estimated to be 3.32 eV for **KGF-24** and 2.94 eV for **KGF-25** from the Tauc plots (Fig. 3b). The absolute valence band maximum (VBM) was evaluated by photoelectron yield spectroscopy (PYS) and the VBM levels of **KGF-24** and **KGF-25** were determined to be −5.15 and −6.12 eV below the vacuum level, respectively (Fig. S8†). Considering the optical band gaps determined using DR-UV-vis spectroscopy, the absolute CBM levels were estimated to be −1.83 eV for **KGF-24** and −3.27 eV for **KGF-25** below the vacuum level (Fig. 3c). The different electronic energy levels of **KGF-24** and **KGF-25** are attributed to the difference in the coordination structure and the $(-Ag-S-)_n$ network.

The photoconductive properties of **KGF-24** and **KGF-25** were investigated by time-resolved microwave conductivity (TRMC) experiments (Fig. 3d). TRMC is a contactless technique that uses high-frequency electromagnetic wave to probe the photo-induced transient conductivity, which provides information regarding the dynamics of photogenerated charge carriers at the multi-nanometer scale.[11] Both **KGF-24** and **KGF-25** exhibited distinct TRMC signals originating from photo-generated charge mobility. The $\varphi\sum\mu_{max}$ (φ = quantum yield of charge-carrier generation; $\sum\mu$ = sum of the hole and electron mobilities) values of **KGF-24** and **KGF-25** were 8.3×10^{-5} and 2.2×10^{-5} cm^2 V^{-1} s^{-1}, respectively. The value of **KGF-24** is comparable to those of other photoconductive CPs and MOFs (Table S2†).[5a,6,12] Excitation intensity dependence of TRMC experiments is presented in Fig. S9.† With decreasing excitation intensity (*ca.* 10^{16}–10^{14} photon cm^{-2} per pulse), the $\varphi\sum\mu_{max}$ of **KGF-24** increased while maintaining the decay rate, suggesting that the charge carrier decay mainly results from charge trapping. As for **KGF-25**, the excitation intensity dependency was not obtained because of a weak signal (Fig. S10†). Overall, since both **KGF-24** and **KGF-25** exhibited TRMC signals with distinct optical band gaps, they qualify as semiconductors.

To gain further insights into the resultant photoconductive nature, first-principles calculations were carried out using the CASTEP software (details of the calculation methods are presented in the ESI†).[13] In the simulated band structure, the band gaps determined by the VBM and CBM were 2.62 eV for **KGF-24** and 1.71 eV for **KGF-25**, consistent with the trends obtained using DR-UV-vis spectroscopy. Notably, the calculated band gaps are typically lower than the experimental values.[14] Both **KGF-24** and **KGF-25** displayed band dispersion parallel to their 2D layer (Z–G, G–Y, A–B, and D–E) in both VBM and CBM (Fig. 4). The dispersion width was in the range 0.2–0.4 eV. Notably, the typical CPs possess a flat band with dispersion widths <0.05 eV because of weak orbital overlapping. Hence, the resulting steep dispersion is a strong indication that the charge transport is remarkable along the 2D layer.

Analysis of the density of states (DOS) provides information regarding the origin of the bands from the elements (the black line represents the total DOS and the other colored lines represent the partial DOS (PDOS)). The PDOS data of **KGF-24** revealed that the VBM largely consists

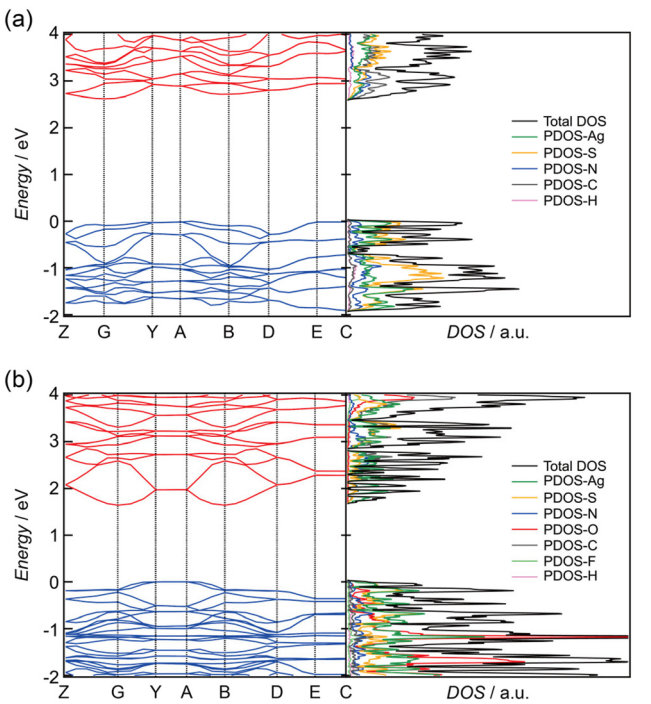

Fig. 4 Band structure and DOS for (a) **KGF-24** and (b) **KGF-25**. The energy level of the VBM is presented as zero in the band structures.

of Ag and S atoms with nearly negligible contributions from the other elements of the $tzdt^-$ anion. The CBM, however, mainly consists of Ag, C, and N atoms with small contributions from the S atom. Mapping for the VBM and CBM demonstrates that the former is delocalized through the $(–Ag–S–)_n$ chain, whereas the latter is mainly localized on C and N atoms (Fig. S11†). In **KGF-25**, the Ag and S atoms also contributed to the VBM and CBM. The mapping shows that the VBM is particularly delocalized throughout the $(–Ag–S–)_n$ structure (Fig. S12†). These results clearly suggest that the $(–Ag–S–)_n$ network in the 2D layer plays a vital role in the resulting photoconductive nature. However, given the fact that **KGF-24** exhibits a higher photoconductivity than **KGF-25** despite its small band dispersion, it is reasonable to assume that the resultant photoconductivity does not originate purely from the band-like charge transport through the $(–Ag–S–)_n$ network, but that it may also be supported by the hopping charge transport.

In conclusion, we selectively obtained 2D semiconductive Ag(I)-based S-CPs, **KGF-24** and **KGF-25**, using the molar ratio of CF_3COOAg and Htzdt. **KGF-24** and **KGF-25** each formed 2D structures with an extended inorganic $(–Ag–S–)_n$ network. The TRMC experiments demonstrated that both **KGF-24** and **KGF-25** are photoconductive. First-principles calculation also revealed that the $(–Ag–S–)_n$ network in the 2D structure contributes to the resulting photoconductivity. Our results undoubtedly provide an additional insight into the fabrication of semiconductive 2D S-CPs.

Author contributions

Ryohei Akiyoshi: investigation, data curation, writing original draft, and funding. Akinori Saeki: TRMC and PYS experiments. Kazuyoshi Ogasawara: theoretical calculations. Hirofumi Yoshikawa: TG analyses. Yuiga Nakamura: single crystal X-ray structural analyses, Daisuke Tanaka: conceptualization and funding.

Conflicts of interest

There are no conflicts to declare.

Acknowledgements

Synchrotron X-ray diffraction experiments on **KGF-24** were performed on BL02B1 beamline at the SPring-8 facility (2022B1583, 2022B1882, and 2022B0521). This work was supported by Grants-in-Aid for Scientific Research (Grant No. JP21K20544, JP22K14702, JP20H05836, and JP20H02577) received from the Japan Society for the Promotion of Science (JSPS). This work was partially supported by JST, CREST Grant Number JPMJCR22O5, Japan. R. A. acknowledges the financial support provided by Hyogo Science and Technology Association, Izumi Science and Technology Foundation, and Kinoshita Memorial Enterprise Foundation. D. T. acknowledges the financial support provided by JST Grant Number JPMJPF2204. We would like to thank Editage (**https://www.editage.jp**) for English language editing.

References

1 (*a*) R. Dong, P. Han, H. Arora, M. Ballabio, M. Karakus, Z. Zhang, C. Shekhar, P. Adler, P. S. Petkov, A. Erbe, S. C. B. Mannsfeld, C. Felser, T. Heine, M. Bonn, X. Feng and E. Canovas, *Nat. Mater.*, 2018, **17**, 1027–1032; (*b*) M. L. Aubrey, B. M. Wiers, S. C. Andrews, T. Sakurai, S. E. Reyes-Lillo, S. M. Hamed, C. J. Yu, L. E. Darago, J. A. Mason, J. O. Baeg, F. Grandjean, G. J. Long, S. Seki, J. B. Neaton, P. Yang and J. R. Long, *Nat. Mater.*, 2018, **17**, 625–632; (*c*) L. S. Xie, G. Skorupskii and M. Dinca, *Chem. Rev.*, 2020, **120**, 8536–8580; (*d*) W.-H. Li, W.-H. Deng, G.-E. Wang and G. Xu, *EnergyChem*, 2020, **2**, 100029.

2 (*a*) A. J. Clough, J. W. Yoo, M. H. Mecklenburg and S. C. Marinescu, *J. Am. Chem. Soc.*, 2015, **137**, 118–121; (*b*) E. M. Miner, L. Wang and M. Dinca, *Chem. Sci.*, 2018, **9**, 6286–6291; (*c*) C. A. Downes, A. J. Clough, K. Chen, J. W. Yoo and S. C. Marinescu, *ACS Appl. Mater. Interfaces*, 2018, **10**, 1719–1727; (*d*) E. M. Miner, T. Fukushima, D. Sheberla, L. Sun, Y. Surendranath and M. Dinca, *Nat. Commun.*, 2016, **7**, 10942.

3 (*a*) M. G. Campbell, S. F. Liu, T. M. Swager and M. Dinca, *J. Am. Chem. Soc.*, 2015, **137**, 13780–13783; (*b*) M. G. Campbell, D. Sheberla, S. F. Liu, T. M. Swager and M. Dinca, *Angew. Chem., Int. Ed.*, 2015, **54**, 4349–4352; (*c*) M. K. Smith and K. A. Mirica, *J. Am. Chem. Soc.*, 2017, **139**, 16759–16767; (*d*) V. Rubio-Gimenez, N. Almora-Barrios, G. Escorcia-Ariza, M. Galbiati, M. Sessolo, S. Tatay and C. Marti-Gastaldo, *Angew. Chem., Int. Ed.*, 2018, **57**, 15086–15090.

4 (*a*) D. Feng, T. Lei, M. R. Lukatskaya, J. Park, Z. Huang, M. Lee, L. Shaw, S. Chen, A. A. Yakovenko, A. Kulkarni, J. Xiao, K. Fredrickson, J. B. Tok, X. Zou, Y. Cui and Z. Bao, *Nat. Energy*, 2018, **3**, 30–36; (*b*) J. Park, M. Lee, D. Feng, Z. Huang, A. C. Hinckley, A. Yakovenko, X. Zou, Y. Cui and Z. Bao, *J. Am. Chem. Soc.*, 2018, **140**, 10315–10323; (*c*) S. S. Shinde, C. H. Lee, J.-Y. Jung, N. K. Wagh, S.-H. Kim, D.-H. Kim, C. Lin, S. U. Lee and J.-H. Lee, *Energy Environ. Sci.*, 2019, **12**, 727–738.

5 (*a*) L. Sun, T. Miyakai, S. Seki and M. Dinca, *J. Am. Chem. Soc.*, 2013, **135**, 8185–8188; (*b*) L. Sun, C. H. Hendon, M. A. Minier, A. Walsh and M. Dinca, *J. Am. Chem. Soc.*, 2015, **137**, 6164–6167; (*c*) R. W. Huang, Y. S. Wei, X. Y. Dong, X. H. Wu, C. X. Du, S. Q. Zang and T. C. W. Mak, *Nat. Chem.*, 2017, **9**, 689–697; (*d*) O. Veselska and A. Demessence, *Coord. Chem. Rev.*, 2018, **355**, 240–270; (*e*) J. Xie, L. Wang and J. S. Anderson, *Chem. Sci.*, 2020, **11**, 8350–8372; (*f*) Y. Kamakura and D. Tanaka, *Chem. Lett.*, 2021, **50**, 523–533; (*g*) G. E. Wang, S. Luo, T. Di, Z. Fu and G. Xu, *Angew. Chem., Int. Ed.*, 2022, **61**, e202203151.

6 T. Wakiya, Y. Kamakura, H. Shibahara, K. Ogasawara, A. Saeki, R. Nishikubo, A. Inokuchi, H. Yoshikawa and D. Tanaka, *Angew. Chem., Int. Ed.*, 2022, **61**, e202203151.

7 (*a*) W. Su, M. Hong, J. Weng, R. Cao and S. Lu, *Angew. Chem., Int. Ed.*, 2000, **39**, 2911–2914; (*b*) O. Veselska, C. Dessal, S. Melizi, N. Guillou, D. Podbevšek, G. Ledoux, E. Elkaim, A. Fateeva and A. Demessence, *Inorg. Chem.*, 2019, **58**, 99–105; (*c*) Y. Li, J. Shu, Q. Huang, K. Chiranjeevulu, P. N. Kumar, G. E. Wang, W.-H. Deng, D. Tang and G. Xu, *Chem. Commun.*, 2019, **55**, 10444–10447; (*d*) H. Jiang, L. Cao, Y. Li, W. Li, X. Ye, W. Deng, X. Jiang, G. Wanga and G. Xu, *Chem. Commun.*, 2020, **56**, 5366–5369; (*e*) Y. Li, X. Jiang, Z. Fu, Q. Huang, G. E. Wang, W. H. Deng, C. Wang, Z. Li, W. Yin, B. Chen and G. Xu, *Nat. Commun.*, 2020, **11**, 261; (*f*) Z. Wu, Q. Yao, Z. Liu, H. Xu, P. Guo, L. Liu, K. Zhang, Z. Lu, X. Li, J. Zhang and J. Xie, *Adv. Mater.*, 2021, **33**, e2006459; (*g*) E. A. Schriber, D. W. Paley, R. Bolotovsky, D. J. Rosenberg, R. G. Sierra, A. Aquila, D. Mendez, F. Poitevin, J. P. Blaschke, A. Bhowmick, R. P. Kelly, M. Hunter, B. Hayes, D. C. Popple, M. Yeung, C. Pareja-Rivera, S. Lisova, K. Tono, M. Sugahara, S. Owada, T. Kuykendall, K. Yao, P. J. Schuck, D. Solis-Ibarra, N. K. Sauter, A. S. Brewster and J. N. Hohman, *Nature*, 2022, **601**, 360–365; (*h*) C. H. Gong, X. Z. Hu, Z. Han, X. F. Liu, M. Z. Yang and S. Q. Zang, *Chem. Commun.*, 2022, **58**, 1788–1791.

8 (*a*) I. G. Dance, K. J. Fisher, R. M. H. Banda and M. L. Scudder, *Inorg. Chem.*, 1991, **30**, 183–187; (*b*) A. A. Levchenko, C. K. Yee, A. N. Parikh and A. Navrotsky, *Chem. Mater.*, 2005, **17**, 5428–5438; (*c*) Z. Ye, L. P. de la Rama, M. Y. Efremov, J. M. Zuo and L. H. Allen, *Dalton Trans.*, 2016, **45**, 18954–18966.

9 (*a*) X.-Y. Wei, W. Chu, R.-D. Huang, S.-W. Zhang, H. Li and Q.-L. Zhu, *Inorg. Chem. Commun.*, 2006, **9**, 1161–1164; (*b*) X. Wei, D. Di, W. Chu, Q. Zhu and R. Huang, *Inorg. Chim. Acta*, 2008, **361**, 1819–1826.

10 M. Jansen, *Angew. Chem., Int. Ed. Engl.*, 1987, **26**, 1098–1110.

11 (*a*) A. Saeki, *Polym. J.*, 2020, **20**, 1307–1321; (*b*) A. Saeki, T. Aida and S. Seki, *Acc. Chem. Res.*, 2012, **45**, 1193–1203.

12 (*a*) T. C. Narayan, T. Miyakai, S. Seki and M. Dinca, *J. Am. Chem. Soc.*, 2012, **134**, 12932–12935; (*b*) T. Okubo, H. Anma, N. Tanaka, K. Himoto, S. Seki, A. Saeki, M. Maekawa and T. Kuroda-Sowa, *Chem. Commun.*, 2013, **49**, 4316–4318; (*c*) Y. Kamakura, P. Chinapang, S. Masaoka, A. Saeki, K. Ogasawara, S. R. Nishitani, H. Yoshikawa, T. Katayama, N. Tamai, K. Sugimoto and D. Tanaka, *J. Am. Chem. Soc.*, 2020, **142**, 27–32; (*d*) Y. Kamakura, C. Sakura, A. Saeki, S. Masaoka, A. Fukui, D. Kiriya, K. Ogasawara, H. Yoshikawa and D. Tanaka, *Inorg. Chem.*, 2021, **60**, 5436–5441; (*e*) Y. Kamakura, S. Fujisawa, K. Takahashi, H. Toshima, Y. Nakatani, H. Yoshikawa, A. Saeki, K. Ogasawara and D. Tanaka, *Inorg. Chem.*, 2021, **60**, 12691–12695.

13 S. J. Clark, M. D. Segall, C. J. Pickard, P. J. Hasnip, M. I. J. Probert, K. Refson and M. C. Payne, *Z. Kristallogr.*, 2005, **220**, 567–570.

14 C. Lee, W. Yang and R. G. Parr, *Phys. Rev. B: Condens. Matter Mater. Phys.*, 1988, **37**, 785–789.

